MAST : a fine mesh transient multiphase code for geothermal fluid networks simulation

Marco Bonizzi[1], Vittorio Faluomi, Paolo Andreussi

[1] TEA Sistemi SPA, Ponte a Piglieri 8, Pisa (PI) Italy CAP 56121

marco.bonizzi@tea-group.com

Keywords: multi-phase flow, pressure-based solver, mono-component fluid.

ABSTRACT

The present paper presents MAST (2009), a transient one-dimensional multi-phase flow simulator for geothermal . From an algorithm view point . From an algorithm view point, the code is entirely based upon a pressure-based solver, whereas from a mathematical framework, the code is based on a multi-field multi-phase flow modelling. From a physical prospective, the mono-component fluid is described on a enthalpy (H) – pressure (P) diagram, which allows the discrimination of the local instantaneous thermodynamic state (i.e. sub-cooled liquid, over-heated vapor, saturation). The MAST code is capable to simulate both mono-branch, complex network, and closed loop systems, and allows to simulate a broad range of piping equipment (i.e. turbines, compressors, heat exchangers, valves, separator, suitable to perform hydraulic studies and a whole geothermal systems. Through the following sections the main physical and numerical framework will be described, as long as some examples of code application to simulate specific geothermal plant phenomena.

1. INTRODUCTION

The main characteristic of the MAST simulator (2009) is encapsulated in a dynamic pattern recognition capability, whereby the different multi-phase flow regimes which can generate (i.e. Stratified, Slug, Dispersed Bubble and Annular) is direct outcome of the numerical solution of the fluid transport governing equations, coupled with the adopted closure relations. MAST adopts a multi-field modelling approach; whereby separate sets of conservation equations are written for each field flowing in the tube. Regardless of the number of phases which are present, the underlying algorithm always remains the same. Each phase present in the domain can travel in two distinct forms: either as a continuous bulk, or a dispersed field; in the former case the continuous field might either entrap some gas bubbles (i.e. liquid film case) or transport liquid droplets (i.e. gas core case). The code can solve for both mono-branch and network cases; moreover, closed loops are also accounted for. Additional available modules cater for the equipment part: to this regard, controllers (i.e. manual, proportional integrative derivative, emergency shut-down, pressure safety vales), valves, pumps, turbines, horizontal gravitational separator, and heat exchanger empower the user in simulating complex geothermal systems.

In what follows, the adopted modelling framework will be presented; then, some relevant results related to various test cases will be presented, and finally conclusions will be drawn.

2. MAST: THE MODELLING FRAMEWORK

In what follows subscripts L, G, D, B, F and C will denote the total liquid phase, total gaseous phase, liquid dispersed field (i.e. liquid Droplets), gas dispersed field (i.e. gas Bubbles), continuous liquid field (i.e. liquid Film), and continuous gas field (i.e. gas Core) respectively. Since the MAST code is a multi-field model, the two (for the present specific case of gas-liquid two-phase flows) distinct layers that can appear will be herein denoted as:

- layer 1, composed of a continuous liquid film with gas bubbles potentially dissolved;
- layer 2, composed of a continuous gas core which can transport liquid droplets.

Let α_L, α_G, α_D, α_B, α_F, and α_C denote the fundamental volume fractions; then the following relations shall hold:

$$\alpha_L = \alpha_D + \alpha_F$$

$$\alpha_G = \alpha_B + \alpha_C$$

$$\alpha_1 = \alpha_F + \alpha_B,\ \alpha_2 = \alpha_C + \alpha_D \quad [1]$$

$$c_B = \frac{\alpha_B}{\alpha_1}, c_D = \frac{\alpha_D}{\alpha_2} \quad [2]$$

The mixture densities associated to layer 1 and 2 immediately follow and their equations is given below.

$$\rho_1 = c_B\ \rho_G + (1 - c_B)\rho_L \quad [3]$$

$$\rho_2 = c_D\ \rho_L + (1 - c_D)\rho_G \quad [4]$$

The adopted notation for the governing conservation equations that will be shortly introduced is as such: *z* and *t* are the spatial and temporal coordinates, α denotes the volume fraction, *k* denotes either layer 1, 2 or 3, *u* is the velocity, g is the gravity acceleration, *P* is the interfacial pressure, *h* the phasic height, τ is the shear stress, ρ the density, *A* is the pipe cross-sectional area, ϑ is the pipe inclination with respect to the horizontal, S_w and S_i denote the wetted perimeter, and the interfacial width respectively, τ_w, and τ_i denote wall and interfacial shear respectively, Ψ is the evaporation condensation mass exchange term, and Φ denotes the mass source term. The mass conservation equations for the total gas, total liquid and the corresponding dispersed fields are written from [5]-[8].

$$\frac{\partial(\alpha_G\rho_G)}{\partial t}+\frac{\partial(\alpha_C\rho_G u_2)}{\partial z}+\frac{\partial(\alpha_B\rho_G u_1)}{\partial z}=\Psi+\Phi_G \qquad [5]$$

$$\frac{\partial(\alpha_L\rho_L)}{\partial t}+\frac{\partial(\alpha_F\rho_L u_1)}{\partial z}+\frac{\partial(\alpha_D\rho_L u_2)}{\partial z}=-\Psi+\Phi_L \qquad [6]$$

$$\frac{\partial(\alpha_B\rho_G)}{\partial t}+\frac{\partial(\alpha_B\rho_G u_1)}{\partial z}=(\Psi+\Phi_G)\frac{\alpha_B}{\alpha_C+\alpha_B}+\phi_{B,E}-\phi_{B,DE} \qquad [7]$$

$$\frac{\partial(\alpha_D\rho_L)}{\partial t}+\frac{\partial(\alpha_D\rho_L u_2)}{\partial z}=(-\Psi+\Phi_L)\frac{\alpha_D}{\alpha_F+\alpha_D}+\Omega_A-\Omega_D \qquad [8]$$

In equation [7] the source $\phi_{B,E}$ and sink $\phi_{B,DE}$ terms denote the gas bubbles entrainment and disengagement rates, of which the closure laws are as follows:

$$\phi_{B,E}=\rho_G A\left[0.076\frac{S_i}{D}(u_w-u_1)-0.15\right]/V \qquad [9]$$

$$\phi_{B,DE}=-\rho_G K\left[1.18\left(\frac{\sigma_{GL}g(\rho_L-\rho_G)}{\rho_L^2}\right)\right]^{0.25}S_i(1-\alpha_1)/V \qquad [10]$$

In equations [9] and [10] V, S_i, u_w and σ_{GL} denote the volume, interfacial chord length, the wave speed and the gas-liquid surface tension. The terms Ω_A and Ω_D represent the droplets atomization and deposition rate respectively; in mathematical terms these two terms are expressed as follows:

$$\Omega_A=\frac{4}{D}\frac{k_A}{\sigma_{GL}}\sqrt{\rho_G\rho_G}u_2^2(\Gamma_F-\Gamma_0) \qquad [11]$$

$$\Omega_D=\frac{4}{D}k_D\frac{\alpha_D}{\alpha_G}\rho_L \qquad [12]$$

In the above equations k_A, k_D, Γ_F and Γ_0 denote the atomization coefficient constant, the deposition velocity coefficient, the liquid film mass flow per circumferential unit length, and a threshold value respectively. More information about the model can be found in Bonizzi et al. (2009). The momentum equations solved in MAST are written for each layer; the generic form of the momentum conservation can be expressed as equation (13) below:

$$\frac{\partial(\alpha_K\rho_K u_K)}{\partial t}+\frac{\partial(\alpha_K\rho_K u_K^2)}{\partial z}=-\alpha_K\frac{\partial P}{\partial z}-\alpha_K\rho_K g\cos(\vartheta)\frac{\partial h_K}{\partial z}+$$
$$-\alpha_K\rho_K g\sin(\vartheta)-\frac{\tau_{wK}S_K}{A}\pm\frac{\tau_i S_i}{A}+\Phi_K u_K \qquad [13]$$

Since MAST is a pressure-based solver, the momentum equations expressed for the two distinct layers, represent a predictor step; new velocity fields for the continuous fields, driven by a newly computed pressure field which satisfies global mass are sought by solution of a density-weighted global mass conservation, which is expressed by equation [14] below

$$\frac{1}{\rho_L}\left[\frac{\partial(\alpha_F\rho_L u_1)}{\partial z}+\frac{\partial(\alpha_D\rho_L u_2)}{\partial z}\right]+\frac{1}{\rho_G}\left[\frac{\partial(\alpha_C\rho_G u_2)}{\partial z}+\frac{\partial(\alpha_B\rho_G u_1)}{\partial z}\right]+\frac{(\alpha_C+\alpha_B)}{\rho_G}\frac{\partial\rho_G}{\partial t}++\frac{(\alpha_D+\alpha_F)}{\rho_L}\frac{\partial\rho_L}{\partial t}=\Psi\left(\frac{1}{\rho_G}-\frac{1}{\rho_L}\right)+\sum_K\frac{\Phi_K}{\rho_K} \qquad [14]$$

Local thermodynamics equilibrium is assumed among the phases; therefore, the energy equation is expressed by a single equation, written in terms of the total mixture enthalpy

$$H_k=c_{p,k}T+\frac{u_k^2}{2}+gY \qquad [15]$$

as shown below:

$$\frac{\partial}{\partial t}(\alpha_G\rho_G H_G+\alpha_L\rho_L H_L)+\frac{\partial}{\partial z}(\alpha_C\rho_G u_2 H_G+\alpha_B\rho_G u_1 H_G+\alpha_F\rho_L u_1 H_L+\alpha_D\rho_L u_2 H_L)-\frac{\partial P}{\partial t}=Q \qquad [16]$$

In equations [15] and [16] above, c_p, *T*, *Y* and *Q* denote the phasic specific heat at constant pressure, the temperature, the elevation and the heat power exchanged across the pipe walls.

2.1 Mono-component module

From a thermodynamics view point, the P (pressure)-T (temperature) plane is to be selected only for identifying the boundaries between the possible states of sub-cooled liquid (identified by the *l* letter in Fig 1), over-heated vapor (identified by the *v* letter in Fig 1), or saturation condition (represented by the continuous line which divides the sub-cooled and over-heater regions). In the present derivation, the pressure-enthalpy plane is rather selected in order to characterize not only the specific thermodynamic state under which the fluid is to be found, but, in case of saturating water, to quantify the equilibrium vapor title for the given instantaneous conditions. For any given mixture enthalpy value at a given pressure, the thermodynamic state can then be immediately identified. If we let $h_{L,SAT}$ and $h_{G,SAT}$ denote the saturation enthalpies for liquid and vapor at the given pressure, from the calculated value of the mixture enthalpy h_M, the thermodynamic state will be derived as shown below.

$$h_M=\begin{cases}if\left(h_M\in[h_{L,SAT},h_{G,SAT}]\right)\rightarrow h_{L,SAT}+\chi\left(h_{G,SAT}-h_{L,SAT}\right)\\ if\left(h_M\le h_{L,SAT}\right)\rightarrow h_L\\ if\left(h_M\ge h_{G,SAT}\right)\rightarrow h_G\end{cases} \qquad [17]$$

As equation [17] clearly indicates, the saturation enthalpies of vapor and liquid must be calculated at the given pressure; then one of the following three conditions will be matched:

a) Saturation state

if the mixture enthalpy is bounded between the liquid and vapor saturation enthalpies, then the water fluid will be under saturated conditions. The vapor thermodynamic can then be derived as follows:

$$\chi = \frac{h_M - h_{L,SAT}}{h_{G,SAT} - h_{L,SAT}} \qquad [18]$$

In equation [18] above the difference between the saturation vapor and liquid enthalpies denotes the latent heat of vaporization and can be briefly indicated as λ. If this condition is satisfied, the temperature shall then correspond to the saturation temperature at the given pressure and the purpose of the energy equation is to provide the value of the vapor title [18];

b) Sub-cooled liquid state

If the mixture enthalpy is upper bounded by the saturation liquid enthalpy at the given pressure, then the thermodynamic state will be sub-cooled liquid and the vapor title will be

$$\chi = 0 \qquad [19]$$

The temperature of the sub-cooled liquid will be derived by applying binary search from the values of the liquid enthalpy at the given pressure.

c) Over-heated vapor state

If the mixture enthalpy is lower bounded by the saturation vapor enthalpy at the given pressure, then the thermodynamic state will be over-heated vapor and the title will be

$$\chi = 1 \qquad [20]$$

The temperature of the over-heated vapor will be derived by applying binary search from the values of the vapor enthalpy at the given pressure.

Knowledge of the instantaneous vapor title is of paramount importance for the calculation of the evaporation/condensation rates. Under saturation condition, the equation which is implemented in MAST is the one expressed by equation [21] below:

$$\Psi = \rho_M \left(\frac{\partial \chi}{\partial t} + u_M \frac{\partial \chi}{\partial z} \right) \qquad [21]$$

In the above equation ρ_M and u_M denote the mixture density and velocity, which can be locally calculated via equations [22] and [23] as follows:

$$\rho_M = \alpha_L \rho_L + \alpha_G \rho_G \qquad [22]$$

$$u_M = (\alpha_C \rho_G u_2 + \alpha_B \rho_G u_1 + \alpha_F \rho_L u_1 + \alpha_D \rho_L u_2)/\rho_M \qquad [23]$$

From a physical view point, meta-stable states (i.e. presence of vapor under sub-cooled liquid conditions, or presence of liquid under over-heated vapor conditions) can temporarily occur, given that the condensation/evaporation are not instantaneous processes; in order to take care of such occurrences from a modelling prospective, ad-hoc rates of condensation and vaporization are defined as follows:

$$\Psi = -\frac{\alpha_G \rho_G}{\Delta t_{COND}} \qquad [24]$$

for the condensation of meta-stable vapor under sub-cooled liquid state thermodynamic condition, and

$$\Psi = +\frac{\alpha_L \rho_L}{\Delta t_{EVAP}} \qquad [25]$$

for the evaporation of meta-stable liquid under over-heated vapor state thermodynamic condition. In the above equations Δt_{COND} and Δt_{EVAP} denote the time required by the condensation and vaporization processes respectively; in the present implementation, those critical times have been taken equal.

2.2 Physical properties calculation

During the validation test cases, it was found that the accuracy in the values of the physical properties of steam and water is extremely important. It is herein felt necessary to remark the fact that no special new modules have been implemented in the code for the instantaneous evaluation of the physical properties for the given values of P and T. The properties of steam and water are supplied via a tabular data or internally generated using Coolprop library; the P-T plane is divided into discrete points, say N points of pressure and N of temperature. In generating the required fluid property file, the user shall prescribe starting (i.e. minimum) values for the pressure and the temperature; interpolation will be used for calculating, at the given pressure and temperature value, the required physical property, by applying equation [26] below:

$$\Phi(P,T) - \Upsilon(P^k,T^k) = \frac{\partial \Upsilon}{\partial P}\Big|_T (P - P^k) + \frac{\partial \Upsilon}{\partial T}\Big|_P (T - T^k) \qquad [26]$$

In the above equation, Φ denotes the physical property to be updated at the given pressure P and temperature T, Υ is the corresponding quantity given in terms of discrete points via the provided file, and the right-hand side terms denote the expansion of the interpolation derivative. Since the multi-component model is heavily dependent upon both P-T and h-P diagrams, it is very important to have well-posed available data related to the Clapeyron equation, which allows to reconstruct the saturation curve in the pressure-temperature plane. These data are indeed provided by the fluid property file, whereby phase change curve pressures at the prescribed discrete temperatures are written. The data are stored into arrays, and for any temperature T value bounded by T1 and T2, or for any pressure value P bounded by P1 and P2, the saturation pressure at the given temperature T or the saturation temperature at the given pressure P will be linearly interpolated. Very importantly, if the property to be evaluated correspond

to a meta-stable phase (i.e. liquid under over-heated thermodynamic conditions, or vapor under sub-cooled liquid thermodynamic conditions), then interpolation points are shifted to the appropriate region corresponding to phase existence.

3. MAST: THE NUMERICAL FRAMEWORK

A standard pressure-velocity coupling scheme (Ferziger and Peric, 1999) is the choice adopted to derive a pressure equation from the global continuity equation (22). The governing equations are numerically discretized on a staggered grid arrangement (Harlow and Welch, 1965) using explicit discretization scheme in time for all equations but the pressure. The adoption of the explicit scheme allows easier parallelization. The time step is limited by the flow Courant number

$$C = \frac{u_{max}\delta t}{\delta z} \qquad [27]$$

In the above equation C, u_{max}, δt and δz denote the Courant number, the maximum phase velocity, the time step size and the mesh spacing respectively. Since the set of model equations is hyperbolic, the boundary conditions have to be prescribed by the characteristics velocity in and out of the flow. In summary, the methodology solves the following equations:

1. Momentum equation of layer 1 – equation [13] [explicitly integrated]
2. Momentum equation of layer 2 – equation [13] [explicitly integrated]
3. Continuity equation of liquid dispersed (droplet) field – equation [7] [explicitly integrated]
4. Continuity equation of gas dispersed (bubbles) field – equation [8] [explicitly integrated]
5. Continuity equation of total liquid phase – equation [6][explicitly integrated]
6. Continuity equation of total gas phase – equation [5] [explicitly integrated]
7. The pressure equation derived equation [14] [implicitly integrated]
8. The energy equation [16] [explicitly integrated].

4. HEAT STRUCTURE MODEL IN MAST

The code enables to simulate the heat exchange between the fluid (i.e. the hydro bound) and the outer environment using an abstraction concept appropriately name heat structure. Within the present work, we shall define a heat structure as a contiguous portion of the computational domain, characterized by the same inner pipe diameter, insulation layers (in terms of thickness and material properties such as heat capacity, thermal conductivity and density), and thermal boundary conditions corresponding to the piping outer environment, which can be chosen to be one of the following: fluid bound, whereby the fluid can either be stagnant or in motion with given properties from which the outer heat transfer coefficient can be computed; soil bound, in order to simulate a buried pipeline; fixed bound, whereby an idealized fluid with prescribed overall heat transfer coefficient and temperature is given, or finally another hydro bound, which allows to simulate the thermal interaction between two portions of the whole fluid computational domain. The heat structures also include the possibility of simulating a fixed power source, which can be either related to a specific layer in the wall or can be homogeneously volumetrically distributed, for investigating the effect of heating or cooling the hydro fluid. It should be remarked that the code also enables the simulation of heat radiative heat transfer. Another relevant characteristic of the MAST code for geothermal applications is the possibility to associate more than one heat structure to the same computational cell; at present, a maximum of up to two heat structures per cell can be given. This feature is deemed to play a quite relevant role in allowing the user to conduct numerical simulations regarding for instance heat exchangers or even complex bundled tubing.

5. EQUIPMENT AND PIPE LINE NETWORKS MODELS IN MAST

The MAST code has various models specifically implementing for the simulation of equipment devices typically encountered in geothermal networks. The following is the list of available models:

- well group: both production and injection are modelled assuming a known production/injection performance of the well (i.e. linear or quadratic forms and tables);
- valves and check valves;
- controllers of various kinds: manual, pressure safety, emergency shutdown, proportional integrative / derivative;
- multiphase flow pumps (with pumps characteristics supplied by the user via either non-dimensional or dimensional quantities);
- booster pumps;
- simplified centrifugal pumps;
- gravitational separator;
- heat exchangers which can be controlled;
- closed loops, converging and diverging networks.

The above described models allow the code to simulate a broad variety of scenarios typically encountered in geothermal plants.

As far as the network simulation capabilities are concerned, it ought to be remarked that the code is capable to simulate both gathering (i.e. converging systems) and distributed (i.e. diverging systems) networks. Besides, the simulator is also capable of simulating a closed loop (which can be, from a topology prospective, prescribed both as mono-branch or network), by implementing periodic boundary conditions which reflect the simulated fluid flow across the section boundary of the last computational cell, and the section boundary of the first one.

6. CODE VALIDATION AND ASSESSMENT

Two assessment phases have been performed with MAST code: an initial separate effect test activity, and a second step regarding phenomenological tests tailored to geothermal applications. A separate effects validation of the MAST code has been performed using

several experimental data coming from different laboratory facilities. The following models were separately assessed:

1. Flow pattern transition
2. Slug characteristic identification
3. Stratified and annular flow pattern pressured drops and liquid level evaluation

6.1 Experimental test evaluation

Flow transition prediction. The robustness of the criteria for identifying the slug transition can be appreciated by looking at **Figure 1**, where the predictions of the critical height of the liquid layer at the transition to slug flow for an air-water flow at atmospheric pressure are plotted against the superficial velocities and compared against the experimental data of Andritsos et al. (1989) and the theoretical transition boundary according to Hurlburt & Hanratty (2002) for a horizontal pipe with 9.53 cm of internal diameter.

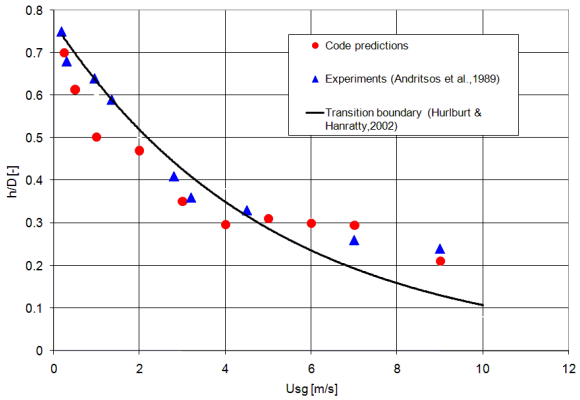

Figure 1: Air-water theoretical predictions, transition data and predictions.

Clearly, the criteria used for identification, again noting that the closure relationships are not adjusted, appear to be accurate. Finally, the code predictions relative to the transition between stratified and slug flows (**Figure 2**) agree very well with the theory and the experiments presented in Taitel & Dukler, (1976).

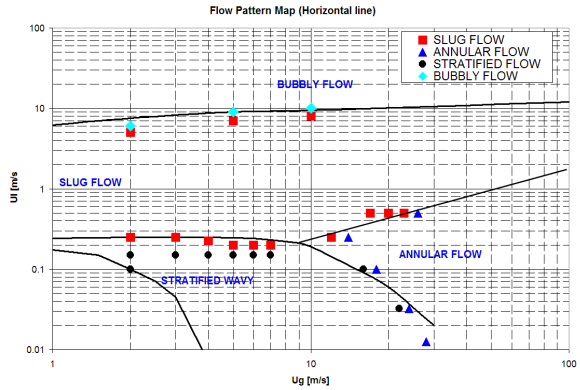

Figure 2: Comparison between MAST flow regime predictions and experimental flow pattern map in a horizontal line

Slug characteristics evaluation. The code has been validated against various data sets, both regarding slug and stratified flow. Some of the results of the validation procedure relative to the slug flow pattern are summarised in **Figure 3** as reported in Andreussi et al. (2008). In Bonizzi et al. (2009) it is also shown that the code not only is able to predict the laboratory measurements of slug length reported in Nydal et al. (1992), but also the standard deviation of these measurements.

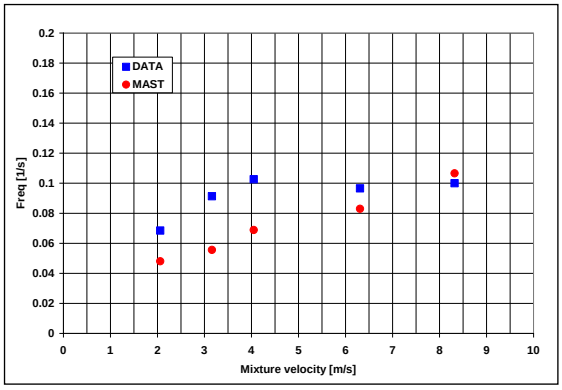

Figure 3 : Comparison of slug frequency between MAST and BHR experimental data

Stratified flow parameters calculation. Concerning stratified flow, the MAST code has been validated using three data sets, namely the data produced by the SESAME project (a R&D activity that was carried out at TEA Sistemi with the support of ENI E&p), Andritsos et al. (1989) and by Ottens et al. (2001). The Errore. L'origine riferimento non è stata trovata. show the fit provided to the present database by some of the correlations available in MAST (Andritsos & Hanratty (1987) and Andreussi & Persen (1987)). In Calgaro et al. (2012) the full validation of the MAST code against stratified data is reported, showing an average accuracy of about 12% in predicting pressure drops and 13% for holdup calculations.

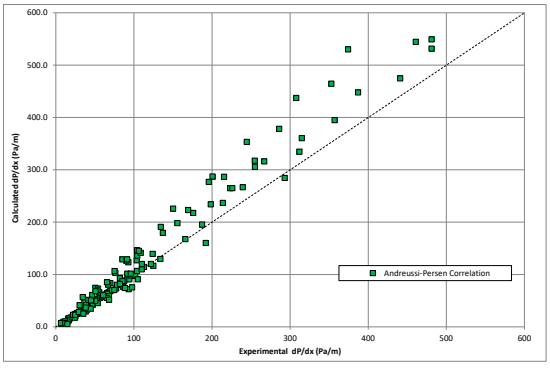

Figure 4 : Calculated vs. experimental pressure gradient: Andreussi-Persen correlation

Annular simplified 2D model. As illustrated in Bonizzi et al. (2016), for horizontal or near-horizontal pipes, the thin liquid film wetting the inner pipe perimeter under stratified-dispersed gas-liquid flow conditions, is modelled taking into account the thinner laminar film which is formed by the deposition of the smaller liquid droplets, and the thicker turbulent liquid film, typically sitting at the pipe bottom, which is

atomized by the fast shearing gas flow leading to droplets entrainment. Finally, in **Figure 5** , the validation of the nearly- 2D film model for annular flow description is reported, showing the good agreement of the proposed model with recorded data.

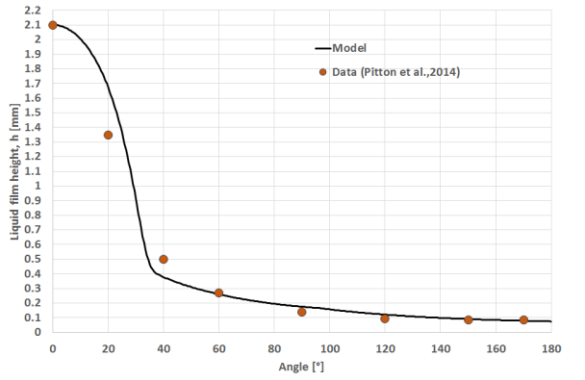

Figure 5: Experimental and calculated liquid film profile thickness across pipe section

6.1 Test cases verification: manometer

As a verification of the capabilities of MAST related to the code application to the geothermal plants, different test cases conceived for the validation and assessment of the code for the specific target are reported hereafter. The first selected test case is a closed (i.e. loop circuit) network composed of 4 branches, each vertically oriented, having each a length of 25m and an inner diameter of 20cm. The simulation gets started with stagnant water having a thermodynamic state corresponding to that of sub-cooled liquid: the bottom pressure is set to 8bar, and the fluid temperature to 35°C. The first two branches (having a combined length of 50m) will be exposed to a hot wall, characterized by a heat transfer coefficient of 1000 [W/(m2K)] and a wall temperature of 60°C, whereas the remaining two branches (having the same combined length of 50m) will be exposed to a cold wall, with the same heat transfer coefficient of 1000 [W/(m2K)] but with a lower wall temperature of 20°C. **Figure 6** shows the conceptual arrangements of the branches.

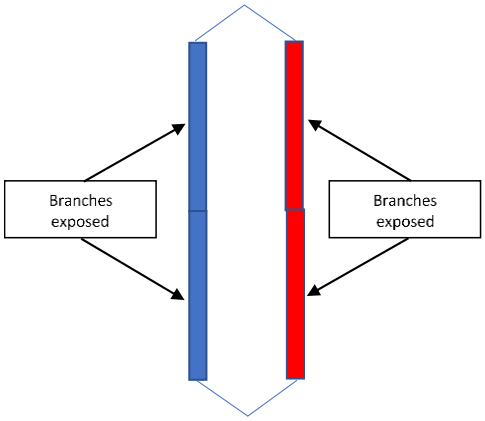

Figure 6 : Sketch of the simulated oscillating manometer.

In order to simulate a closed loop, the boundaries are reflected between the first centroid of the computational domain which relates to the first branch of the loop, and the last centroid of the computational domain related to the last branch of the loop. Of course, the same shall apply for the trivial mono-branch case: in this case the boundaries would be simply reflected between first and last computational cell. In particular, the outlet (i.e. imposed at the last cell of the domain) pressure shall always (i.e. during both time and iteration levels) equate the inlet (i.e. calculated at the first cell of the domain) pressure, and the inlet mass flow rates, phase velocities and volume fractions will be taken from the calculated (volume fractions, vapor title and temperature) or extrapolated (outlet velocities) at the ghost cell related to the last cell of the computational domain. An interesting aspect of the given test case is that, assuming the outlet/inlet temperature T_{IN} to be known, it is possible to derive a theoretical equation from the energy balance applies to the two distinct (i.e. the first exposed to a hot wall, the second to a cold one) regions of the domain, which allows to calculate, from the prescribed boundary conditions, the mass flow rate (assuming a thermodynamic state of either sub-cooled liquid or over-heated vapor). The equation is expressed as follows:

$$m_K = \mathrm{K}\frac{\mathrm{A}-\mathrm{B}}{2(c_K(\mathrm{B}+\mathrm{A})-\mathrm{E})} \qquad [28]$$

where the terms are calculated as follows:

$$\mathrm{K} = \pi D L h_\infty, \mathrm{A} = T_H - T_{IN}/2, \mathrm{B} = T_C - T_{IN}/2, \mathrm{E} = c_K T_{IN} \qquad [29]$$

In equations [28] and [29] m_K, D, L, h_∞, T_H, c_K and T_C denote the mass flow rate of phase k (be it either liquid or vapor), the pipe diameter, the length of the region (in the present case 50m), the overall heat transfer coefficient, the temperature of the hot wall, the heat capacity at constant pressure of phase k, and the temperature of the cold wall respectively. Feeding inlet temperature values in the expected range, the derived mass flow rate versus inlet temperature curve, based in entirety upon equation [35], is illustrated in **Figure 7**.

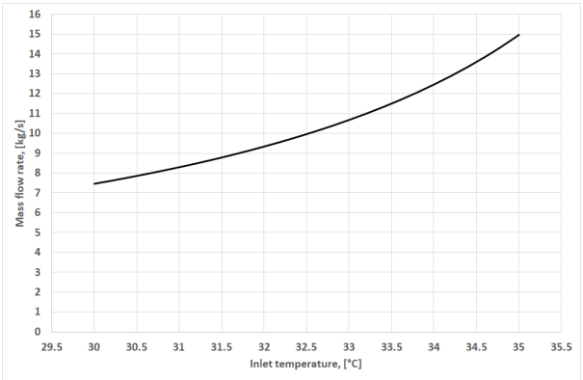

Figure 7: Flowrate vs. inlet temperature calculated for thermal manometer inlet

The simulation has been carried out using a mesh size corresponding to 10 pipe diameters; the code predicts that the thermodynamic state of the entire closed loop corresponds to a sub-cooled liquid state, with water

flowing at a rate corresponding to approximately 9.9kg/s. The resulting pressure and temperature profiles are shown in **Figure 8** below.

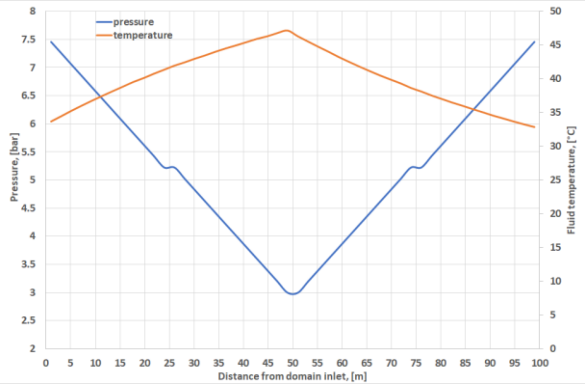

Figure 8: Pressure and temperature profiles in thermal oscillating manometer

6.2 Test cases verification: Cavitation in water pipe

The second test case relates to a typical cavitation investigation. The domain corresponds to a partially submerged piping system which is found downstream of a pump. Aim of the simulation is to simulate the effect of an ocean's wave on the fluid contained within the pipe. In order to simulate the effect of the wave, transient pressure boundary conditions shall apply at the domain outlet as it will be explained in what follows. The line is roughly 130m long and the inner diameter corresponds to 35cm; the adopted numerical mesh spacing corresponds to 5 pipe diameters**. Figure 9** illustrates the line altimetry, whereby the X and Y values indicate the position of any given point in a XY Cartesian plane. The boundary conditions correspond

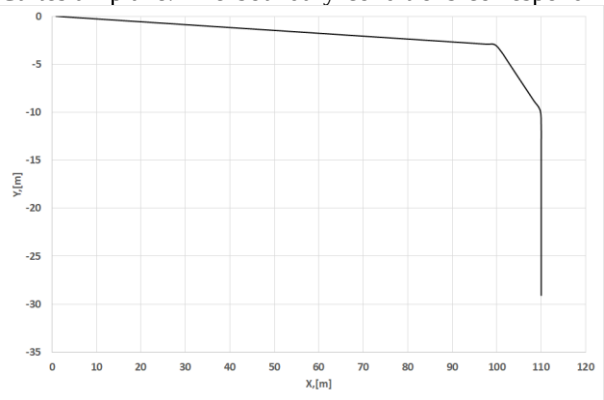

Figure 9: Line altimetry XY for cavitation investigation study.

to a closed node (no inflow/outflow can occur) at pipe inlet and equate to 3bar absolute pressure at the pipe bottom for almost the entire simulation duration, besides 14 seconds when the pressure will abruptly decrease to 1.2bar and rise to 3bar again; this fast event wants to mimic the effect of a wave hitting the pipe. The water and vapor flow fields are initialized such that, in the first 100m long portion of the pipe, the volume fraction of stagnant water is 100%, and in the submerged part of the line the volume fraction of water is 90%. The initial fluid temperature is set to around 50°C and at that temperature the thermodynamic state is found to be sub-cooled liquid. As soon as the pressure drops to 1.2 bar, at the top of the submerged water pipe, where the pressure even when only liquid is present is anyhow below atmospheric, the pressure will drop even more, eventually the diminishing pressure will intersect the saturation curve, leading to bubbles formation and coalescence; nonetheless the transient applies to a 12 seconds time span only: the system will start to oscillate between thermodynamic states characterized by the appearance and disappearance of saturation regions until the whole of the system goes back to the thermodynamic state of sub-cooled liquid as it was the case before the sudden depressurization (which mimics a wave's effect). **Figure 10** shows the traces of the total vapor volume in the entire line).

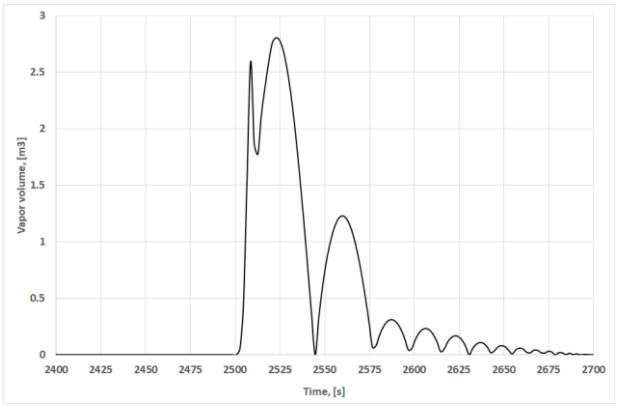

Figure 10: Vapor traces as transient outlet pressure conditions kick-in.

The **Figure 11** illustrate the system responds to the sudden change in P conditions by sucking water (i.e. in liquid state of course) into the domain from the domain exterior, releasing the entrained water back to the outlet, and the process will repeat itself at weaker rate until the pressure wave dies out and the entire system achieves the stagnant fluid condition under thermodynamic state of sub-cooled liquid again.

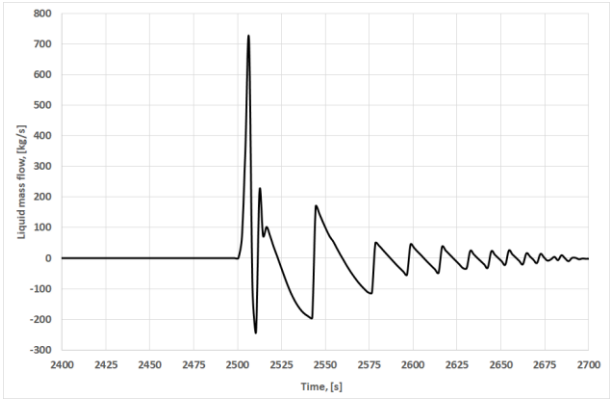

Figure 11: Vapor traces as transient outlet pressure conditions kick-in.

When the pressure wave travels from the pipe inlet to the pipe outlet, the bulk pressure drops change and vapor can subsequently form as bubbles. **Figure 12** captures such occurrence, and moreover displays the

profiles of the bulk pressure along the line and the calculated saturation pressure at the given temperature

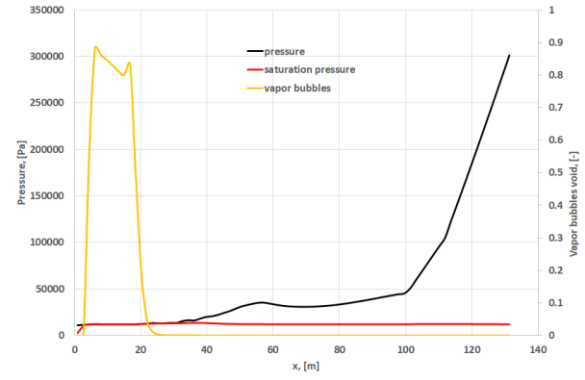

Figure 12: Vapor bubbles, static and saturation pressure profiles after the transient.

CONCLUSIONS

The present document illustrates the mathematical, modelling and numerical framework implemented within the MAST code, a transient one-dimensional multi-phase flow simulator which allows simulation of complex geothermal networks, both for design and for management and production optimization activities. The software has the capabilities to simulate in detail the development of a mono-component mixture (water and vapor) along a geothermal pipeline network and plant, made possible by the implementation of an ad-hoc mono-component module, and by a broad selection of available pipeline equipment modules, such as valves, controllers, check-valves, pumps, separators and heat exchangers. The code allows the simulation of different systems: simple mono-branch flow lines, closed circuits and mode complex networks (both converging and diverging), covering most of the actual geothermal plants available in production, as well as the new implementations including OCR or combined plants, like geothermal coupled with thermodynamic solar. Presently, the code has been validated sing a large database of laboratory data, and some field data have been used to verify the code accuracy for overall production system. Further validation using data coming from geothermal plants have been already planned, to extend and further validate the code accuracy specifically for geothermal applications.

REFERENCES

Bonizzi, M., Andreussi, P. Banerjee S., 2009 "**Flow regime independent, high resolution, multi-field modelling of near horizontal gas-liquid flows in pipelines**" *Int. J. Multiphase Flow*, **35**, 34-46.

Ferziger. J.H. & Peric, M. 1999, **Computational methods for fluid dynamics**. Springer, Germany.

Harlow, F.H. & Welch, J.E. 1965 "**Numerical calculation of time-dependent viscous incompressible flow of fluid with free surface**". *Phys. Fluids* **8**, 2182-2189.

Andreussi, P. & Persen, L.N. 1987 "**Stratified gas-liquid flow downwardly inclined pipes**". *Int. J. Multiphase Flow* **13**, pp. 565-575.

Taitel, Y., Dukler, A.E. 1976 "**A model for predicting flow regime transitions in horizontal and nearly horizontal gas-liquid flow**" *J. AIChE* **22**, pp. 47-55

Andritsos, N. & Hanratty, T.J. 1987 "**Influence of interfacial waves in stratified gas-liquid flows**" *J. AIChE*. **33**, pp. 444-454.

Andritsos N., Williams, L. & , Hanratty, T.J. 1989 "**Effect of liquid viscosity on the stratified-slug transition in horizontal pipe flow**" *Int. J. Multiphase Flow* **15**, pp. 877-892

Hurlburt, E.T., Hanratty, T.J. 2002 "**Prediction of the transition from stratified to slug and plug flow for long pipes**" *Int. J. Multiphase Flow* **28**, pp. 707-729.

Andreussi P., Bonizzi M., Di Lullo A., Margarone M. 2008 "**Advanced simulation of gas-liquid pipelines**" 6th *North American Conference BHR, Banff, Canada*

Nydal, O.J., Pintus, S., Andreussi, P. 1992 "**Statistical characterization of slug flow in horizontal pipes**" *Int. J. Multiphase Flow* **18**, pp. 439-453.

Andritosos, N., "**Effect of Pipe Diameter and Liquid Viscosity on Horizontal Stratified Flow**", *Ph. D. Thesis*, Univ. Ilinois, Urbana, 1986

Ottens, M., Hoefsloot, H.C.J., Hamersma, P.J., "**Correlations Predicting Liquid Hold-up and Pressure Gradient in Steady State (Narly) Horizontal Co-current Gas-Liquid Pipe Flow**". *Trans. IChemE*, **79**, pp. 581-592, 2001.

Calgaro, B., Andreussi, P., Bonizzi, M., Faluomi, V., Margarone, M., Ellul, I. 2012 "**Simulation of stratified gas-liquid flow in near-horizontal pipes**" *PSIG Annual Meeting, Santa Fe, New Mexico*, 15-18 May.

Bonizzi, M., Andreussi, P. 2016 "**One-dimensional model of wet gas flow in near-horizontal pipes**" *BHR North American Conference, Banff, CA*